



Impact of multiple radar reflectivity data assimilation on the numerical simulation of a flash flood event during the HyMeX campaign

Ida Maiello^{1,2}, Sabrina Gentile^{3,1}, Rossella Ferretti², Luca Baldini⁴, Nicoletta Roberto⁴, Errico Picciotti^{2,5}, Pier Paolo Alberoni⁶, and Frank Silvio Marzano^{1,2}

¹Department of Information Engineering, Electronics and Telecommunications, Sapienza University of Rome, Rome, Italy

²CETEMPS, Department of Physical and Chemical Sciences, University of L'Aquila, L'Aquila, Italy

³Institute of Methodologies for Environmental Analysis, CNR IMAA, Potenza, Italy

⁴Institute of Atmospheric Sciences and Climate, CNR ISAC, Rome, Italy

⁵Himet s.r.l., L'Aquila, Italy

⁶Arpa Emilia Romagna, Servizio Idro-Meteo-Clima, Bologna, Italy

Correspondence to: Ida Maiello (ida.maiello@aquila.infn.it)

Received: 23 June 2016 – Discussion started: 15 July 2016

Revised: 19 August 2017 – Accepted: 26 September 2017 – Published: 7 November 2017

Abstract. An analysis to evaluate the impact of multiple radar reflectivity data with a three-dimensional variational (3-D-Var) assimilation system on a heavy precipitation event is presented. The main goal is to build a regionally tuned numerical prediction model and a decision-support system for environmental civil protection services and demonstrate it in the central Italian regions, distinguishing which type of observations, conventional and not (or a combination of them), is more effective in improving the accuracy of the forecasted rainfall. In that respect, during the first special observation period (SOP1) of HyMeX (Hydrological cycle in the Mediterranean Experiment) campaign several intensive observing periods (IOPs) were launched and nine of which occurred in Italy. Among them, IOP4 is chosen for this study because of its low predictability regarding the exact location and amount of precipitation. This event hit central Italy on 14 September 2012 producing heavy precipitation and causing several cases of damage to buildings, infrastructure, and roads. Reflectivity data taken from three C-band Doppler radars running operationally during the event are assimilated using the 3-D-Var technique to improve high-resolution initial conditions. In order to evaluate the impact of the assimilation procedure at different horizontal resolutions and to assess the impact of assimilating reflectivity data from multiple radars, several experiments using the Weather Research

and Forecasting (WRF) model are performed. Finally, traditional verification scores such as accuracy, equitable threat score, false alarm ratio, and frequency bias – interpreted by analysing their uncertainty through bootstrap confidence intervals (CIs) – are used to objectively compare the experiments, using rain gauge data as a benchmark.

1 Introduction

In the last few years, a large number of floods caused by different meteorological events have occurred in Italy. These events mainly affected small areas (few hundreds of square kilometres) making their forecast very difficult. Indeed, one of the most important factors in producing a flash flood was found to be the persistence of the meteorological system over the same area in the presence of specific hydrological conditions (the size and the topography of the drainage basin, the amount of urban use within the basin, and so on), allowing for the accumulation of a large amount of rain (Doswell et al., 1996). In complex orography areas, such the Italian regions, this is largely due to the barrier effect produced by the mountains, such as the Apennines. Moreover, the Mediterranean Basin is affected by a complex meteorology, due to

Impact of Multiple Doppler Radar data assimilation on the numerical simulation of a Flash Flood Event during the HyMeX campaign

I. Maiello¹, S. Gentile¹, R. Ferretti^{1,2}, L. Baldini³, N. Roberto³, E. Picciotti^{4,1}, P.P. Alberoni⁵, F. S. Marzano^{6,1}

¹Centre of Excellence CETEMPS, Department of Physics and Chemistry - University of L'Aquila, L'Aquila, Italy

²Danish Meteorological Institute, Copenhagen, Denmark

³Institute of Atmospheric Sciences and Climate, CNR ISAC, Roma, Italy

⁴Himet s.r.l, L'Aquila, Italy

⁵Arpa Emilia Romagna - Servizio Idro-Meteo-Clima, Bologna, Italy

⁶Department of Electronic Engineering, Sapienza University of Rome, Rome, Italy

Correspondence to: Ida Maiello (ida.maiello@aquila.infn.it)

Abstract. An analysis to evaluate the impact of assimilating multiple radar data with a three dimensional variational (3D-Var) system on a heavy precipitation event is presented. The main goal is to establish a general methodology to quantitatively assess the performance of flash-flood numerical weather prediction at mesoscale. In this respect, during the first Special Observation Period (SOP1) of HyMeX (Hydrological cycle in the Mediterranean Experiment) campaign several Intensive Observing Periods (IOPs) were launched and nine occurred in Italy. Among them IOP4 is chosen for this study because of its low predictability. This event hit central Italy on 14 September 2012 producing heavy precipitation and causing several damages. Data taken from three C-band radars running operationally during the event are assimilated to improve high resolution initial conditions. In order to evaluate the impact of the assimilation procedure at different horizontal resolution and to assess the impact of assimilating multiple radars data, several experiments using Weather Research and Forecasting (WRF) model are performed. Finally, the statistical indexes as accuracy, equitable threat score, false alarm ratio and frequency bias are used to objectively compare the experiments, using rain gauges data as benchmark.

Keywords: radar data assimilation, WRF, 3D-Var, HyMeX

1 Introduction

The scientific community widely recognized the need for high resolution numerical weather prediction (NWP) models to improve the very short term forecast of severe weather events and flash floods. The combination of NWP and weather radar observations has shown improved skill with respect to extrapolation-based techniques (Sun et al., 2014). However, the reliability of the mesoscale NWP models is largely dependent on the initial and lateral boundary conditions (IC and BC), and at the resolution of kilometers even more critical because of the lack of high resolution observations, beside for radar data. Several studies in the meteorological area have shown that the assimilation of appropriate observations into the NWP models, especially radar (Sugimoto et al., 2009) and satellite data (Sokol 2009),

36 significantly reduces the "spin-up" effect (Daley 1991) and improves the IC and BC of the mesoscale models. Classical
37 observations such as SYNOP (surface synoptic observations) or TEMP (upper level temperature, humidity, and winds
38 observations) have not enough density to describe for example local convection, while radar measurements can provide
39 a sufficient density of data. Maiello et al. (2014) showed the positive impact of the radar data assimilation into the
40 precipitation forecast of a heavy precipitation event in Central Italy. The authors showed the gain by using assimilating
41 radar data with respect to the conventional ones. Similar results are obtained for a case of severe convective storm in
42 Croatia by Stanesic and Brewster (2015).

43 Weather radar plays a key role in revealing tridimensional structures of convective storms and the related mesoscale and
44 microscale systems (Nakatani, 2015). Xiao and Sun (2007) showed that assimilating radar data into the NWP models at
45 high resolution (2km), the convective systems could be better represented in the model initial conditions. Recent
46 investigations from the meteorological perspective have shown that the assimilation of real-time observations,
47 especially the radar measurements (reflectivity or/and Doppler velocity), into the mesoscale NWP models can improve
48 the rainfall forecast for the next few hours (e.g. Xiao et al., 2005; Sokol and Rezacova, 2006; Stephan et al., 2008;
49 Dixon et al., 2009; Salonen et al., 2010).

50 This study aims at investigating the potential of improving the NWP rainfall forecasts by assimilating multiple radars
51 data. This may have a direct benefit also for hydrological applications, particularly for real time flood forecasting. The
52 novelty of this paper is in exploring impact on the high resolution forecast of the assimilation of multiple radars data in
53 complex orography area such the Italian region to predict intense precipitation. This aim is reached by using the IOP4
54 of the SOP1 of the HyMeX campaign. The SOP1 was held from 5 September to 5 November 2012; the IOP4 was issued
55 for the Central Italy (CI) target area on 14 September 2012 and it was tagged both as a Heavy Precipitation Event (HPE)
56 and a Flash Flood Event (FFE). Radar reflectivity from three C-band Doppler weather radars is assimilated together
57 with traditional meteorological observations (SYNOP and TEMP) using 3D-Var to improve the Weather Research and
58 Forecasting (WRF) model performance.

59 The paper is organized as follows. Section 2 provides information on the case study and all the observations to be
60 assimilated by WRF 3D-Var. Section 3 introduces the configuration of the WRF model and the functions of the WRF
61 3D-Var data assimilation system. The results are presented and evaluated in Section 4. Finally, summary and
62 concluding remarks are given in Section 5.

63 **2 Study area and data**

64
65 The HyMeX project (<http://www.hymex.org>) aims at a better understanding of the water cycle in the Mediterranean
66 with emphasis on extreme weather events. The observation strategy of HyMeX is organized in a long-term (4 years)
67 Enhanced Observation Periods (EOP) and short-term (2 months) Special Observation Periods (SOP). During the SOP1,
68 that was held from 5 September to 5 November 2012, three Italian hydro-meteorological site were identified within the
69 Western Mediterranean Target Area (TA): Liguria–Tuscany (LT), northeastern Italy (NEI) and central Italy (CI).

70 **2.1 Case study**

71
72 During IOP4 a deep trough entered the Tyrrhenian Sea slowly moving south eastward. Advection of cold air along the
73 central Adriatic coast occurred producing instability over central and southern Italy, and enhanced the Bora flow over
74 the northern Adriatic Sea. The heavy precipitations occurred in the morning of September 14 mainly along the central

75 eastern Italian coast (Marche and Abruzzo regions), associated with the cut-off low over the Tyrrhenian Sea (Figure 1a,
76 c). This structure lasted until 15th September (Figure 1b, d).

77 Figure 2 shows the interpolated map of 24h accumulated rainfall recorded from rain gauges network from September
78 14th to September 15th (00:00-00:00UTC) with a maximum accumulated rainfall on the highest peak of Abruzzo region
79 approximately reaching 300 mm in 24hours. DEWETRA is an operational platform used by the Italian Civil Protection
80 Department (DPC) and designed by CIMA Research Foundation to support operational activities at national or
81 international scale. Rain gauges time series of some selected stations in Marche and Abruzzo regions where most of
82 rainfall is accumulated during the event are presented in Figure 3: Fermo and Pintura di Bolognola (Marche region)
83 respectively with nearly 130 mm/24h (Figure 3a) and 180 mm/24h (Figure 3b), Campo Imperatore, Atri and Pescara
84 Colli (Abruzzo region) with respectively nearly 300mm/24h (Figure 3c), 160 mm/24h (Figure 3d) and 140 mm/24h
85 (Figure 3e). It is clearly shown (Figure 3) that the incremental accumulation started around 02:00UTC of 14th
86 September: in Fermo, Atri and Pescara Colli most of rainfall was concentrated in the first half of the day, whereas in
87 Pintura di Bolognola and Campo Imperatore, precipitation fell all day long.

88 It is worthwhile to point out the large amount of hourly precipitation for Pescara and Atri respectively at 05:00UTC and
89 06:00UTC (red ovals in Fig. 3e and 3d respectively) reaching 45mm/h, indicating convective precipitation, whereas the
90 precipitation on the Gran Sasso (Fig. 3c) was much weaker but lasting longer which allowed for reaching an
91 accumulated amount of 300mm/24h.

92 Figure 4 reports a graphical tool that combines the Vertical Maximum Intensity (VMI) reflectivity from the Italian radar
93 network (Vulpiani et al., 2008a) together with the Meteosat Second Generation (MSG) 10.8 μm image (in normalized
94 inverted greyscale). VMI values above 45 dBZ are associated with intense precipitation occurred during convective
95 events. Zoom over CI target area shows a line of convective cells along the Apennines in Central Italy due to western
96 flow approaching the orographic barrier.

97

98 **2.2 Observations to be assimilated**

99 Conventional observations SYNOP and TEMP were retrieved from the ECMWF Meteorological Archival and Retrieval
100 System (MARS). A total of 989 observations (967 SYNOP and 22 TEMP) are ingested into the coarse resolution
101 domain, whereas a total of 338 (331 SYNOP and 7 TEMP) observations are ingested into the high resolution one.

102 Volumetric reflectivity taken from three C-band Doppler radars operational during the IOP4 have been assimilated to
103 improve IC. Radars have different technical characteristics and were operated with different scanning strategies and
104 operational settings. Data from the single polarization Doppler Mt. Midia radar (MM, 42°03'28" N, 13°10'38"E,
105 h=1760m ASL, n°elevations=4, temporal resolution=15 min, range resolution=500 m) are provided by the Centro
106 Funzionale of Abruzzo Region. The data from the dual polarization Doppler Polar 55C radar (POL, 41° 50' 24" N, 12°
107 38' 50"E, h=102 m ASL, n°elevations=6 or 8, temporal resolution=5 min, range resolution=75 m) are provided by
108 ISAC-CNR of Rome; finally, data from the dual polarization Doppler San Pietro Capofiume radar (SPC, 44°23'24"N,
109 11°22'12"E, h=31m ASL, n°elevations=6, temporal resolution=15 min, range resolution=250 m) are provided by Arpa
110 Emilia Romagna. MM and SPC radars are included in the Italian radar network, while Polar 55C is a research radar
111 working on demand which was operational during HyMeX IOPs (Roberto et al., 2016).

112 It is well known that radar observations can be affected by several sources of errors, mainly due to ground clutter,
113 attenuation due to propagation or beam blocking, anomalous propagation and radio interferences. For this reason, a
114 preliminary procedure to correct acquired radar reflectivity from the three radars is applied before the assimilation
115 procedure consisting of the following 2 steps:

- 116 • pre-processing consists of a first quality check of radar volumes where radar pixel affected by ground clutter
117 and anomalous propagation were filtered. Furthermore, Z was corrected for attenuation using a methodology
118 based on the specific differential phase shift (K_{dp}) available for dual polarization radars (Vulpiani et al, 2015);
- 119 • conversion to the model format is applied to all radars data.

120

121 **3 Methodology and sensitivity analysis design**

122

123 The numerical weather prediction experiments are performed in this work using the Advanced Research WRF model
124 Version 3.4.1. WRF is a non-hydrostatic, primitive-equation, mesoscale meteorological model with advanced dynamics,
125 physics and numerical schemes, where the sigma coordinates are adopted to describe the vertical levels. Detailed
126 descriptions of the model can be found in Skamarock et al. (2008) and also on the WRF user website
127 (<http://www2.mmm.ucar.edu/wrf/users/>). WRF set up, advanced implementation and numerical investigations for flash
128 flood forecast are described in this section

129

130 **3.1 WRF model set up**

131 In this study, a configuration using two domains run independently is used: a 12km domain (263x185) that covers
132 central Europe and west Mediterranean basin (referred as D01) is initialized using the European Centre for Medium-
133 Range Weather Forecasts (ECMWF) analyses at 0.25 degrees of horizontal resolution; an innermost domain, that covers
134 the whole Italy (referred as D02), with a grid space of 3 km (445x449) using as BC and IC the output of the previous
135 forecast at 12km. Both domains run with 37 unequally spaced vertical levels, from the surface up to 100 hPa (Figure 5).

136 The WRF model has options for different physical parameterizations such as the boundary layer, the convection and
137 radiation schemes, etc. The performance of a mesoscale model is highly dependent on the parameterization schemes,
138 especially convection, which might be suitable for one ‘storm type’ but inappropriate for another. The main physics
139 packages used in these experiments are set as for the operational configuration used at CETEMPS (Ferretti et al., 2014),
140 which include (Skamarock et al., 2008): the “New” Thompson et al. 2004 microphysics scheme, the Mellor-Yamada-
141 Janjic scheme for the planetary boundary layer, the Goddard shortwave radiation scheme and the rapid radiative transfer
142 model longwave radiation scheme, the Eta similarity scheme for the description of the surface layer and the Noah Land
143 Surface Model to present the land surface physics. A few preliminary tests are performed to assess the best cumulus
144 parameterization scheme to be used both for the coarse and finest resolution domain for this event. Hence the following
145 parameterizations are tested: the new Kain-Fritsch, and the Grell 3D scheme, which is an improved version of the
146 Grell-Deveneyi scheme that may also be used on high resolution (only on coarser domain in our simulations) if
147 subsidence spreading (option `cugd_avedx`) is turned on. Based on the results of these two cumulus parameterization
148 schemes, the one producing the best precipitation forecast will be used to investigate the impact of the data assimilation.

149

150 3.2 3D-Var data assimilation system

151

152 Data assimilation is the technique by which observations are combined with a NWP product (called the *first guess* or
153 *background forecast*) and their respective error statistics to provide an improved estimate (named the *analysis*) of the
154 atmospheric (or oceanic) state (Skamarock et al., 2008). The variational data assimilation technique achieves this
155 through the iterative minimization of a prescribed cost function (or penalty) (Ide et al., 1997):

156

$$157 J(\mathbf{x}) = J^b(\mathbf{x}) + J^o(\mathbf{x}) = \frac{1}{2}\{[\mathbf{y}^o - H(\mathbf{x})]^T \mathbf{R}^{-1}[\mathbf{y}^o - H(\mathbf{x})] + (\mathbf{x} - \mathbf{x}^b)^T \mathbf{B}^{-1}(\mathbf{x} - \mathbf{x}^b)\}, \quad (1)$$

158

159 where \mathbf{x} is the unknown analysis state vector, found by minimizing the cost function $J(\mathbf{x})$, \mathbf{x}^b is the first guess state
160 vector of the NWP model, \mathbf{y}^o is the assimilated observation vector and $\mathbf{y}=H(\mathbf{x})$ is the forward model derived observation
161 transformed from the analysis \mathbf{x} by the observation operator H for comparison against \mathbf{y}^o .

162 The minimization of the cost function $J(\mathbf{x})$, shown by Equation (1), represents a posteriori maximum likelihood
163 (minimum variance) estimate of the true atmosphere state, given the two sources of a priori data: the first guess \mathbf{x}^b and
164 the observation vector \mathbf{y}^o (Lorenc, 1986). The fit to individual observation points is weighted by the estimates of their
165 errors, i.e. \mathbf{B} and \mathbf{R} , which are the background covariance error matrix and the observation covariance error matrix,
166 respectively.

167 The 3D-Var system developed by Barker et al. (2003, 2004) is used in this study in tandem with the WRF model for
168 assimilating radar reflectivity and the conventional observations SYNOP and TEMP. Its configuration is based on an
169 incremental formulation of the variational problem, producing a multivariate incremental analysis for pressure, wind,
170 temperature and relative humidity in the model space. The incremental cost function minimization is performed in a
171 preconditioned control variable space. The preconditioned control variables are stream function, unbalanced potential
172 velocity, unbalanced temperature, unbalanced surface pressure and pseudo relative humidity. In the case of additional
173 assimilation of the radar reflectivity, the total water mixing ratio q_t is chosen as the moisture control variable instead of
174 pseudo relative humidity. The following Equation (2) shows the observation operator used to calculate the model-
175 derived reflectivity for the comparison with the observed one (Sun and Crook, 1997):

176

$$177 Z = 43.1 + 17.5 \log(\rho q_r), \quad (2)$$

178 where Z is the co-polar radar reflectivity factor in dBZ, ρ is the air density in kg/m^3 and q_r is the rainwater mixing ratio.
179 Since the total water mixing ratio q_t is used as the control variable, the partitioning of the moisture and hydrometeor
180 increments is necessary during the minimization procedure. A warm rain parameterization (Dudhia, 1989) is adopted in
181 WRF 3D-Var, exploiting a constraint based on the relation among rainwater, cloud water, moisture and temperature.
182 When rainwater information, through the reflectivity factor expression in Equation (2), enters the minimization iteration
183 procedure, the forward warm rain process and its backward adjoint distribute the information to the increments of other
184 variables under the constraint of the warm rain parameterization scheme.

185 The performance of the data assimilation system largely depends on the goodness of the background error covariance
186 (BEC), that is the matrix \mathbf{B} in Equation (1). In this study, a domain specific background error statistics is generated
187 based on the forecast data from the same domain. The background errors are applied to the same set of the control
188 variables, stream function, unbalanced potential velocity, unbalanced temperature, unbalanced surface pressure, and

189 pseudo-relative-humidity. Furthermore, the control variables are in eigenvector space and uses an empirical orthogonal
190 function (EOF) to represent the vertical covariance. The background error covariance matrix is generated via the
191 National Meteorological Center (NMC) method (Parrish and Derber, 1992) for both domains. To estimate the NMC-
192 based error statistics, two forecasts are performed every day for the entire SOP1 period (5 September - 5 November
193 2012): a 24h forecast (starting from 00:00UTC) and a 12h forecast (starting from 12:00UTC) valid at the same time.
194 The differences between the two forecasts at t+24 and t+12 are used to calculate the domain-averaged error statistics.

195
196

3.3 Design of the numerical experiments

197 The simulations on the coarser resolution domain (D01) are run from 12:00UTC of 13 September 2012 and integrated
198 for the following 96 hours, whereas runs on the finest resolution domain started at 00:00UTC of September 14 for a
199 total of 48 hours of integration. The 00:00UTC coarser resolution WRF forecast is used as the first guess (FG) in the
200 3D-Var experiment that is the analysis time in the assimilation procedure. After assimilation, the lateral and lower
201 boundary conditions are updated for the high resolution forecast. Finally, the new initial and boundary conditions are
202 used for the model initialization (in a warm start regime) at 00:00UTC. As already pointed out a set of preliminary
203 experiments are performed using different cumulus convective scheme to assess the best one to be used. The following
204 experiments are performed without assimilation and using the convective scheme on the coarser resolution domain
205 only: KAIN-FRITSCH (KF_MYJ); GRELL3D (GRELL3D_MYJ); GRELL3D associated to the CUGD factor
206 (GRELL3D_MYJ_CUGD). A summary of these numerical experiments is given in Table 1.

207 The analysis of the results of these set of experiments allows establishing the best model configuration for the radar data
208 assimilation experiments. The data assimilation (DA) experiments aim to investigate:

- 209 1. the impact of the assimilation at low and high resolution by assimilating both conventional and non-
210 conventional data at both resolutions;
- 211 2. the impact of the assimilation of different types of observations;
- 212 3. the impact of the different radars, which is investigated by performing experiment by assimilating conventional
213 data and then adding radar one by one.

214 The following experiments are performed: i) the control simulation (CTL) without data assimilation; the assimilation of
215 conventional data (SYNOP and TEMP) only (CON_LR_12KM); ii) the assimilation of radar data from MM only
216 (CONMM_LR_12KM) are added; iii) the assimilation of POL radar is added to the previous experiments
217 (CONMMPOL_LR_12KM); iv) the assimilation of the third radar data is added to the previous
218 (CONMMPOLSPC_LR_12KM). Finally, an experiment to assess the role of the outer loop is performed
219 (CONMMPOLSPC3OL_LR_12KM). The multiple outer loops strategy (Rizvi et al., 2008) allows for including non-
220 linearity in the observation operators and for assessing the influence of observations entering for each cycle. The non-
221 linear problem is solved iteratively as a sequence of linear problems by running more than one analysis outer loop, so
222 the assimilation system is able to ingest more observations. The experiments are summarized in (Table 2).

223 The MET (Model Evaluation Tools) application (DTC, 2013), developed at the DTC (Developmental Testbed Center,
224 NCAR), has been used to objectively evaluate the 12 hours accumulated precipitation produced by WRF on the high
225 resolution domain. The observations used for the statistical evaluation were obtained from the Platform DEWETRA of
226 the Department of Civil Protection and the comparison has been performed over the central Italy target area using about
227 3000 rain gauges with a good cover throughout the area.

228

229 **4 Results and discussion**

230

231 In this section the results will be presented and discussed following the rationale of the previously introduced
232 experiments and using statistical indexes for performance quantitative assessment.

233

234 **4.1 Sensitivity test to cumulus parameterization**

235 The 24h accumulated rainfall on Central Italy simulated by the model both on D01 (left column) and D02 (right
236 column) using a different cumulus parameterization scheme (Fig. 6, on line 1 Kain-Fritsch, on line 2 Grell 3D, on line 3
237 Grell 3D and `cugd_avedx=3` activated) is shown. Comparing the model outputs (Fig. 6) and the rain gauge observations
238 (Fig. 2), it is worth noting that best performance on D01 is obtained by Grell 3D which is able to simulate the peak
239 precipitation cumulated in 24 hour (between 200 and 300 mm) over Gran Sasso (Fig. 6, lines 2 and 3), whereas Kain-
240 Fritsch (Fig. 6a) completely misses the peak of rainfall on Abruzzo region (red spot in Fig. 2). Moreover, the rainfall
241 pattern is not properly reproduced.

242 Furthermore results suggest that the spreading of the convective downdraft over several grid points allows for
243 improving the rainfall distribution at both resolution: both the main cells of heavy rainfall are correctly separated over
244 Abruzzo both on D01 and D02 (Fig. 6e and 6f) and the rainfall pattern along the northeast coast of Abruzzo region is
245 also reproduced (Fig. 6f). The statistical indices computed using MET are showed in the next figure. The MET
246 statistical analysis support the previous finding: the GRELL3D_MYJ_CUDG (blue curve Fig. 7) in the range 5-30
247 mm/12h shows higher performances in terms of accuracy (ACC, Fig 7a), equitable threat score (ETS, Fig. 7b) and false
248 alarm ratio (FAR, Fig. c) than the other two simulations. Also the frequency bias (FBIAS, Fig. 7d, green and blue
249 curves) indicates the simulations performed with Grell 3D as the one producing better results. Indeed it shows values
250 closer to 1 (the best value) than Kain-Fritsch (red curve). Finally, the mean error (ME, Fig. 7e, blue curve) for Grell 3D
251 with `cugd_avedx` activated has values close to 0 (perfect value).

252 Here after GRELL3D_MYJ_CUDG is referred as the control (CTL) experiment performed without any data
253 assimilation. Therefore, a new set of simulations are performed following the previous strategies: data assimilation on
254 low or high resolution domains or on both domains simultaneously; conventional data and/or radar data assimilation.

255

256 **4.2 Impact of conventional and radar data assimilation on rainfall forecast: low versus high resolution**

257 In figure 8 a preliminary comparison among the low resolution (12km) simulations is shown. The control simulation
258 (CTL) without data assimilation is shown in Figure 8a; whereas the other panels show the experiments performed using
259 the data assimilation.

260 Observing the outputs of different experiments (Fig. 8) listed in Table 2, best simulation is found for
261 CONMMPOLSPC_LR_12KM (Fig.8e) for which an attempt to reproduce the rainfall maximum over Campo
262 Imperatore (black arrow) is found: the rainfall amount is very well simulated, however a cell displacement is noticeable.
263 Furthermore a quite good attempt to forecast precipitation along the coasts (black oval) is also found.

264 The statistical indices (Fig. 9) support this finding: the brown curve (CONMMPOLSPC_LR_12KM) is producing the
265 best ACC and FAR for all thresholds, except for ETS where good values are found only for thresholds lower than 20
266 mm/12h.

267 Similarly to the above comparison, high resolution results are presented in figure 10 obtained performing data
268 assimilation only on 12km domain (column 1), only on 3km (column 2) and both on 12km and 3km (column 3); to the
269 top of figure 10 the CTL experiment on D02 is shown. Figure 10 is organized as follows: viewing panels by line on line
270 1 all the simulations with conventional data assimilation (CON*) only are found; on line 2 all the experiments with the
271 assimilation of the data from Mt. Midia radar added (CONMM*); on line 3 all the experiments with the assimilation of
272 the data from 2 C-band radars added (CONMMPOL*); on line 4 all the experiments with the assimilation of the data
273 from all 3 C-band radars added (CONMMPOLSPC*); on line 5 the simulations where the strategy of outer loop is
274 adopted (CONMMPOLSPC3OL*). For these experiments the values of the main statistical indices (ACC, FBIAS, ETS,
275 FAR) have been summarized over tables reporting only two thresholds of precipitation: 1 mm/12h and 20 mm/12h
276 (light and heavy rain regimes).

277 To the aim of investigating the impact of the assimilation at different resolutions, we start analyzing figure 10 by
278 column and comparing it with the observation (fig. 2); the statistical analysis is also used:

- 279 • column 1 (12KM): CTL produces an overestimation of the rainfall that is not corrected by the assimilation of
280 conventional data, but assimilating the 3 radars and introducing the 3 outer loops (Fig. 10 column 1 line 4) the
281 main cells are better reproduced. MET indices in Table 3 suggest that CTL and
282 CONMMPOLSPC3OL_HR_12km are the simulations with the best response, secondly CONMM_HR_12KM;
- 283 • column 2 (3KM): a partial correction of the rainfall overestimation compared to column 1 is observed
284 especially if all the radars are assimilated and the outer loop strategy is applied; the statistical indices in Table
285 4 show CONMMPOLSPC3OL_3KM as the best experiment among the assimilated ones;
- 286 • column 3 (12KM_3KM): rainfall overestimation was partially corrected compared to columns 1 and 2 by all
287 experiments; the MET statistics in Table 5 shows that CTL and CONMMPOLSPC3OL_3KM_12KM are the
288 experiments that return better values.

289 Summarizing, the previous analysis suggests that the frequency of rainfall overestimation for higher thresholds has been
290 reduced by radar data assimilation performed only on DOM1. Furthermore, improvements come out for heavy rain
291 regimes when radar data assimilation has been performed on the highest resolution domain, whereas the ingestion of
292 conventional observations produces the worst results since a smaller number of them were assimilated into the finest
293 resolution domain than that the coarser one. The assimilation, operated on both 12 km and 3 km, gives better results
294 than the ones on column 1, but a response worse than the others on column 2 is given for higher thresholds.

295 To the aim of investigating the impact of the assimilation of different data and radars, we can now analyze the
296 experiments showed in figure 10 by line. The results are compared with the observations of Fig. 2. The following
297 considerations are worth discussing:

- 298 • line 1 (CON): a strong reduction of the rainfall is found with respect to CTL if conventional data are
299 assimilated, but the rainfall pattern remains unchanged; statistical indices in Table 6 seem do not improve
300 performances of CTL. The indices values suggest a slightly better performance when the conventional
301 observations are assimilated only on the bigger domain;

- 302 • line 2 (CONMM): a further reduction in the precipitation overestimation is found as well as some variations in
303 the pattern of the rainfall; statistics in Table 7 shows that Mt. Midia radar data assimilation improves model
304 performance above all for higher thresholds; conventional observations assimilation in tandem with MM gives
305 better results;
- 306 • line 3 (CONMMPOL): a quite strong improvement in the rainfall amount is found for all simulations. From the
307 statistics of Table 8 we have found a worsening of the results especially for heavy rain regimes when POL is
308 added (FBIAS and ETS); a better answer is given by the simulation where assimilation is performed on both
309 domains;
- 310 • line 4 (CONMMPOLSPC): a clear correction of the rainfall pattern is found; the overestimation produced by
311 the simulation where all the radars are assimilated on the 3km domain has been corrected by the experiment in
312 which the radars are assimilated both on D01 and D02; statistical indices in Table 9 suggest that the addition of
313 SPC radar improves the results, furthermore they are not better than those where only MM is ingested;
- 314 • line 5 (CONMMPOLSPC3OL): the outer loop experiments confirms the overestimation reduction by
315 *12KM_3KM; from Table 10 it seems that the introduction of 3OL improves the indices values above all
316 when the 12km domain is considered; CONMMPOLSPC3OL_12KM_3KM can be considered the best
317 simulation.

318

319 In summary, simulations results show that it is better to perform the assimilation of conventional observations on the
320 lowest resolution domain. Regarding the assimilation of radar data, POL is the one that gives the worst results due to
321 significant errors in rainfall detection and thus misleading the WRF model forecast. The outer loop strategy could have
322 an important role in the assimilation procedure, but this latter needs a further investigation because a general rainfall
323 underestimation for higher thresholds is found.

324

325 **5 Conclusions**

326 The purpose of this paper has been to assess the impact of multiple radar data assimilation on a heavy precipitation
327 event occurred during the SOP1 of the HyMeX campaign. A sensitivity study at different domain resolution and using
328 different types of data to improve initial conditions has been performed by assimilating into the WRF model radar
329 reflectivity measurements, collected by three C-band Doppler weather radars operational during the event that hit
330 Central Italy on 14 September 2012. The 3D-Var and MET are the WRF tools used to assess this purpose. First of all,
331 WRF model responses to different type of cumulus parameterization have been tested to establish the best configuration
332 and to obtain the control simulation. The latter has been compared with observations and other experiments performed
333 using 3D-Var. The set of assimilation experiments have been conducted following two different strategies: (i) data
334 assimilation at low and high resolution or at both resolutions simultaneously; (ii) conventional data against radar data
335 assimilation. Both have been examined to assess the impact on rainfall forecast.

336 The major findings of this work have been the following:

- 337 • Grell 3D parameterization improves the simulations both on D01 and D02 and the use of the spreading factor is
338 an added value in properly predict heavy rainfall over inland of Abruzzo and the rainfall pattern along the
339 northeast coast;

- 340 • investigating the impact of the assimilation at different resolutions, best results are showed by the experiments
341 where the data assimilation is performed on both domains 12km and 3km;
- 342 • the impact of the assimilation using different types of observations shows improvements if all the radars
343 together with conventional data are assimilated; furthermore MM is the one that better impact the model
344 results because of it has been better detected the event;
- 345 • the outer loop strategy allows for further improving positive impact of the assimilation of multiple radars.
346 Moreover, a deeper investigation of multiple outer loops strategy is required to assess its impact.

347 Analyzing the results obtained in this study, it is not possible to assess which is, in general, the best model configuration
348 since this analysis should be performed systematically with a significant number of case studies. However, this is work
349 is providing a general approach that can encourage to investigate more flash-flood cases in order to make the
350 assimilation of multiple radars data suitable for operational use. In order to confirm and consolidate these initial
351 findings, apart from analyzing more case studies, a "pseudo-operational" testing would be also useful.

352

353 **Acknowledgements**

354 We are grateful to the Gran Sasso National Laboratories for computing resources support, as well as the National Civil
355 Protection Department and CIMA Research Foundation for rain gauges data using for the model validation. National
356 Center for Atmospheric Research is also acknowledge for WRF model and 3D-Var system.

357

358 **References**

359

360 Barker, D.M., Huang, W., Guo, Y.-G., and Bourgeois, A.: A Three-Dimensional Variational (3D-Var) Data
361 Assimilation System For Use With MM5. NCAR Tech. Note, NCAR/TN-453+STR, UCAR Communications, Boulder,
362 CO, 68pp, 2003.

363 Barker, D.M., Huang, W., Guo, Y.-R., Bourgeois, A., and Xiao, Q.: A Three-Dimensional Variational (3D-Var) Data
364 Assimilation System For Use With MM5: Implementation and Initial Results. *Mon. Wea. Rev.*, 132, 897-914, 2004.

365 Daley, R.: Atmospheric Data Analysis, Cambridge University Press, Cambridge, UK, 1991.

366 Developmental Testbed Center, 2013: MET: Version 4.1 Model Evaluation Tools Users Guide. Available at
367 <http://www.dtcenter.org/met/users/docs/overview.php>. 226 pp.

368 Dixon, M., Li, Z., Lean, H., Roberts, N., and Ballard, S.: Impact of data assimilation on forecasting convection over the
369 United Kingdom using a high-resolution version of the Met Office Unified

370 Model, *Mon. Weather Rev.*, 137, 1562–1584, 2009.

371 Dudhia, J.: Numerical study of convection observed during the winter monsoon experiment using a mesoscale two-
372 dimensional model, *J. Atmos. Sci.*, 46, 3077–3107, 1989.

373 Ferretti, R., E. Pichelli, S. Gentile, I. Maiello, D. Cimini, S. Davolio, M. M. Miglietta, G. Panegrossi, L. Baldini, F.
374 Pasi, F. S. Marzano, A. Zinzi, S. Mariani, M. Casaioli, G. Bartolini, N. Loglisci, A. Montani, C. Marsigli, A. Manzato, A.

375 Pucillo, M. E. Ferrario, V. Colaiuda, and R. Rotunno: Overview of the first HyMeX Special Observation Period over
376 Italy: observations and model results. *Hydr. Earth Syst. Sci.*, 18, 1953–1977, 2014, doi:10.5194/hess-18-1953-2014,
377 2014.

378 Ide, K., Courtier, P., Ghil, M., and Lorenc, A. C.: Unified notation for data assimilation: Operational, sequential and
379 variational, *J. Meteorol. Soc. Jpn.*, 75, 181–189, 1997.

380 Li Y., Wang X., and Xue M., 2008: Assimilation of radar radial velocity data with the WRF ensemble-3DVAR hybrid
381 system for the prediction of hurricane Ike, *Mon. Wea Rev.*, vol. 140, pp. 3507–3524.

382 Lorenc, A. C.: Analysis methods for numerical weather prediction, *Q. J. Roy. Meteorol. Soc.*, 112, 1177–1194, 1986.

383 Maiello, I., Ferretti, R., Gentile, S., Montopoli, M., Picciotti, E., Marzano, F. S., and Faccani, C.: Impact of radar data
384 assimilation for the simulation of a heavy rainfall case in central Italy using WRF–3DVAR, *Atmos. Meas. Tech.*, 7,
385 2919–2935, doi:10.5194/amt-7-2919-2014, 2014.

386 Nakatani T., Misumi R., Shoji Y., Saito K., Seko H., Seino N., Suzuki S-I., Shusse Y., Maesaka T., and Sugawara H. ;
387 Tokyo metropolitan area convection study for extreme weather resilient cities. *BAMS*, 96, ES123–ES126, 2015.

388 Parrish, D.F. and Derber, J.C.: The National Meteorological Center’s Spectral Statistical-Interpolation Analysis System.
389 *Mon. Wea. Rev.*, 120, 1747–1763, 1992.

390 Rizvi, S., Guo, Y.-R., Shao, H., Demirtas, M., and Huang, X.-Y.: Impact of outer loop for WRF data assimilation system
391 (WRFDA). 9th WRF Users' Workshop, Boulder, Colorado, 23–27 June 2008.

392 Roberto, N., Adirosi, E., Baldini, L., Casella, D., Dietrich, S., Gatlin, P., Panegrossi, G., Petracca, M., Sanò, P., and
393 Tokay, A.: Multi-sensor analysis of convective activity in central Italy during the HyMeX SOP 1.1, *Atmos. Meas.*
394 *Tech.*, 9, 535–552, doi:10.5194/amt-9-535-2016, 2016.

395 Salonen K, Haase G, Eresmaa R, Hohti H, Järvinen H. 2010. Towards the operational use of Doppler Radar radial
396 winds in HIRLAM. *Atmospheric Research* 100: 190–200.

397 Skamarock, W.C., Klemp, J.B., Dudhia, J., Gill, D.O., Barker, D.M., Duda, M. G., Huang, X.-Y., Wang, W., and
398 Powers, J. G.: A description of the Advanced Research WRF Version 3. NCAR Technical Note. TN 475+STR, 113
399 pp., available from www.mmm.ucar.edu/wrf/users/docs/arw_v3.pdf (last access: January 2012), 2008.

400 Sokol, Z. and Rezacova, D.: Assimilation of Radar reflectivity into the LMCOSMO model with a high horizontal
401 resolution, *Meteorol. Appl.*, 13, 317–330, 2006.

402 Sokol, Z.: Effects of an assimilation of Radar and satellite data on a very short range forecast of heavy convective
403 rainfalls, *Atmos. Res.*, 93, 188–206, 2009.

404 Stanesic A., and K.A. Brewster: Impact of Radar Data Assimilation on the Numerical Simulation of a Severe Storm in
405 Croatia. *Met.Zeit.* DOI 10.1127/metz/2015/0574, 2015.

406 Stephan K, Klink S, Schraff C. 2008. Assimilation of Radar derived rain rates into the convective scale model COSMO-
407 DE at DWD. *Quarterly Journal of the Royal Meteorological Society* 134: 1315–1326.

408 Sugimoto, S., Crook N.A., Sun J., Xiao Q., and Barker D.M., 2009: An examination of WRF 3D-Var Radar data
409 assimilation on its capability in retrieving unobserved variables and forecasting precipitation through observing system
410 simulation experiments. *Mon. Wea. Rev.*, 137, 4011–4029, DOI:10.1175/2009MWR2839.1.

411 Su, J. Xue, M., Wilson J. W., Zawadzki I., Ballard S.P., Onvlee-Hooimeyer J., Joe P., Barker D.M., Li P-W., Golding
412 B., Xu M., and Pinto J.: Use of NWP for nowcasting convective precipitation, recent progress and challenges. *BAMS*,
413 95, 409-426, 2014.

414 Sun, J. and Crook, N.A.: Dynamical and Microphysical Retrieval from Doppler RADAR Observations Using a Cloud
415 Model and Its Adjoint. Part I: Model Development and Simulated Data Experiments. *J. Atmos. Sci.*, 54, 1642-1661,
416 1997.

417 Thompson, G., R. M. Rasmussen, and K. Manning, 2004: Explicit forecasts of winter precipitation using an improved
418 bulk microphysics scheme. Part I: Description and sensitivity analysis.
419 *Mon. Wea. Rev.*,132, 519–542.

420 Vulpiani G., Pagliara, P., Negri, M., Rossi, L., Gioia, A., Giordano, P., Alberoni, P. P., Cremonini, R., Ferraris, L., and
421 Marzano, F. S.: The Italian radar network within the national early-warning system for multi-risks management, Proc.
422 of Fifth European Conference on Radar in Meteorology and Hydrology (ERAD 2008), 184, Finnish Meteorological
423 Institute, Helsinki, 30 June-4 July, 2008a.

424 Vulpiani, G., Baldini, L., and Roberto, N.: Characterization of Mediterranean hail-bearing storms using an operational
425 polarimetric X-band radar, *Atmos. Meas. Tech.*, 8, 4681-4698, doi:10.5194/amt-8-4681-2015, 2015.

426 Wang X., Barker D. M., Snyder C., and Hamill T. M., 2008: “A hybrid ETKF-3DVAR data assimilation scheme for the
427 WRF model. Part I: observation system simulation experiment,” *Monthly Weather Review*, vol. 136, no. 12, pp. 5116–
428 5131.

429 Xiao, Q., Kuo, Y.-H., Sun, J. and Lee, W.-C.: Assimilation of Doppler RADAR Observations with a Regional 3D-Var
430 System: Impact of Doppler Velocities on Forecasts of a Heavy Rainfall Case. *J. Appl. Meteor.*,44, 768-788, 2005.

431 Xiao, Q. and Sun, J.: Multiple-RADAR Data Assimilation and Short-Range Quantitative Precipitation Forecasting of a
432 Squall Line Observed during IHOP_2002. *Mon. Wea. Rev.*, 135, 3381-3404, 2007.

433

434

435

436

437

438

439

440

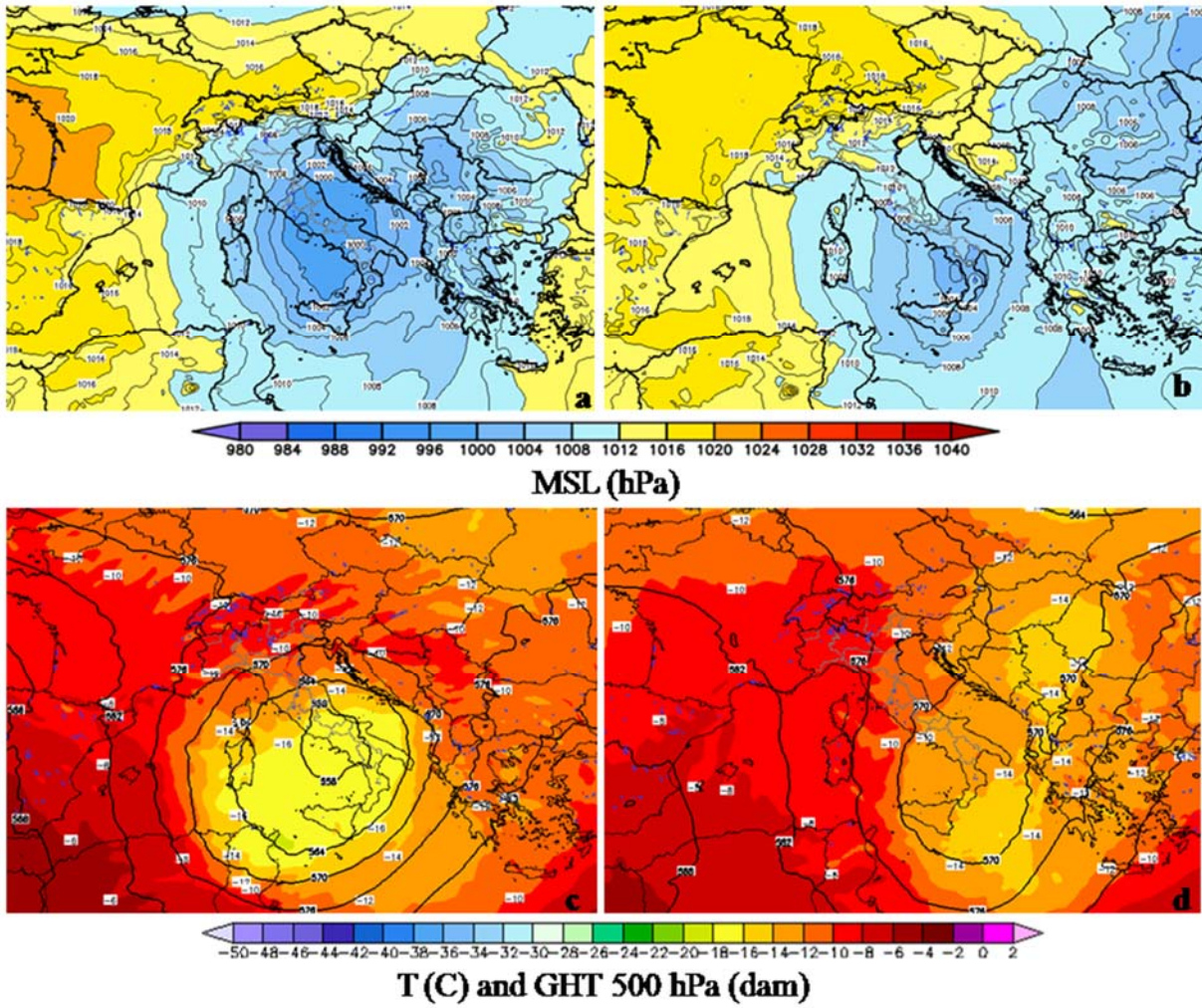
441

442

443

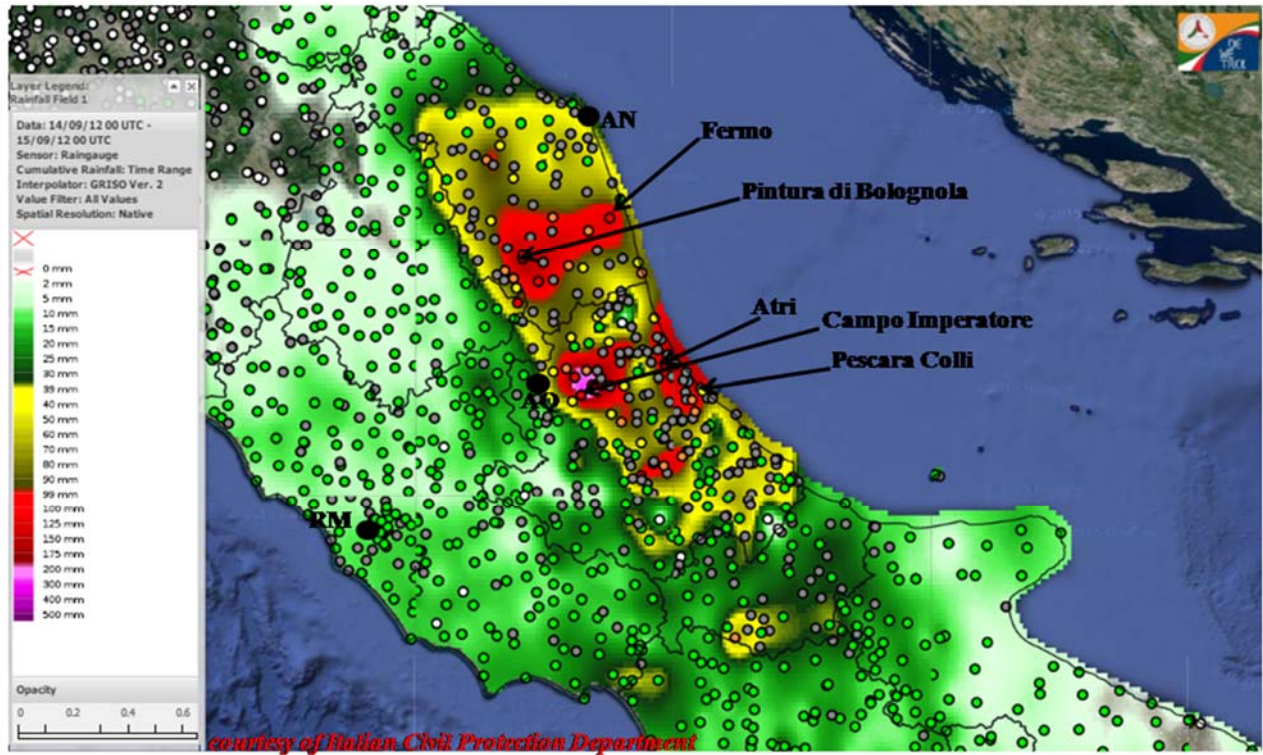
444
445

LIST OF FIGURES



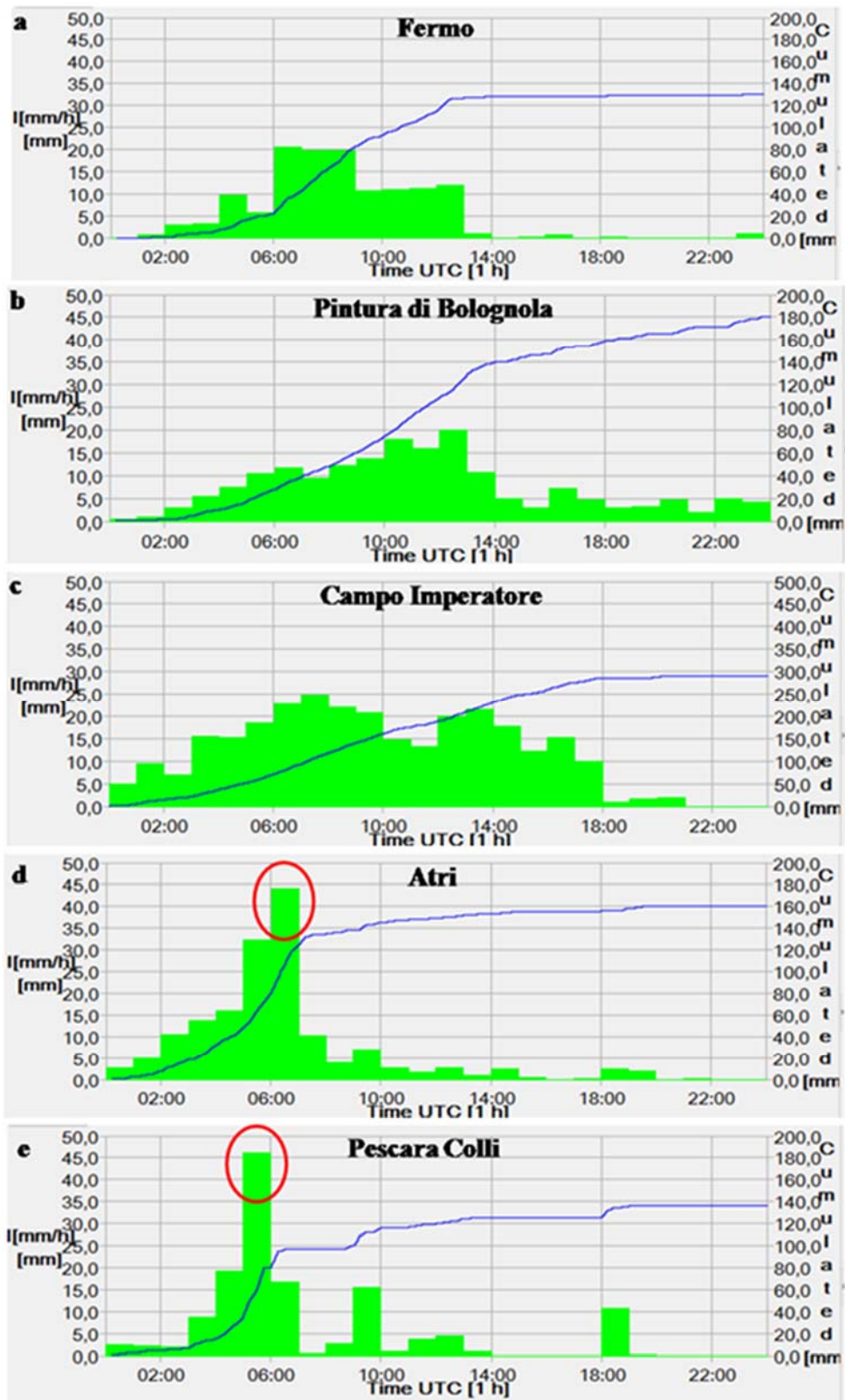
446
447
448
449
450

Figure 1: Mean sea level pressure (a, b), temperature and geopotential height at 500 hPa (c, d) at 12:00UTC on 14 September and 15 September 2012, respectively.



451
 452
 453
 454
 455

Figure 2: Interpolated map of 24h accumulated rainfall from 00:00 UTC of 14 September 2012 over Abruzzo and Marche regions from DEWETRA system obtained by rain gauges measurements. Black contours are the administrative boundaries of Regions.



456

457

458

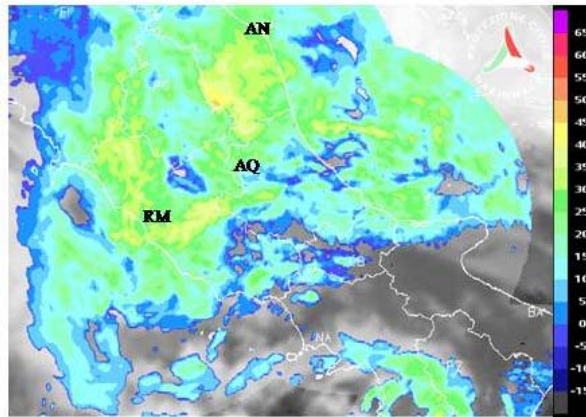
459

460

461

462

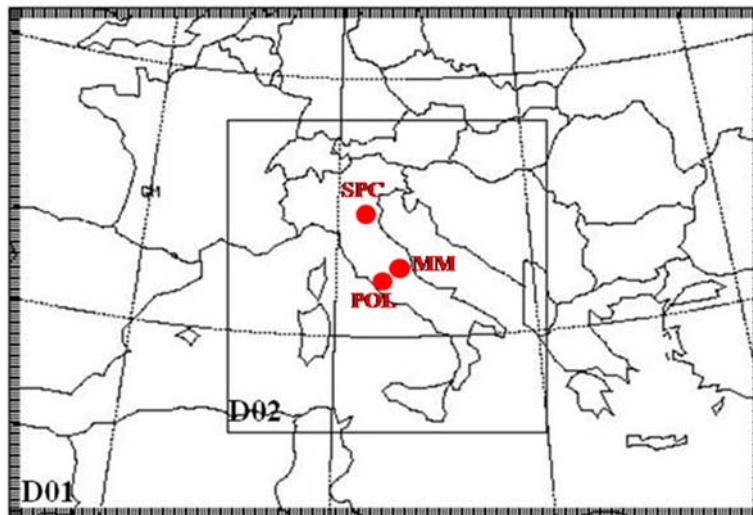
Figure 3: Rain gauges time series of some selected stations in Marche (a and b) and Abruzzo (c, d and e) regions during the event on 14 September 2012. The green histogram represents the hourly accumulated precipitation (scale on the left); the blue line represents incremental accumulation within the 24h (scale on the right). (courtesy of Italian Civil Protection Department)



463

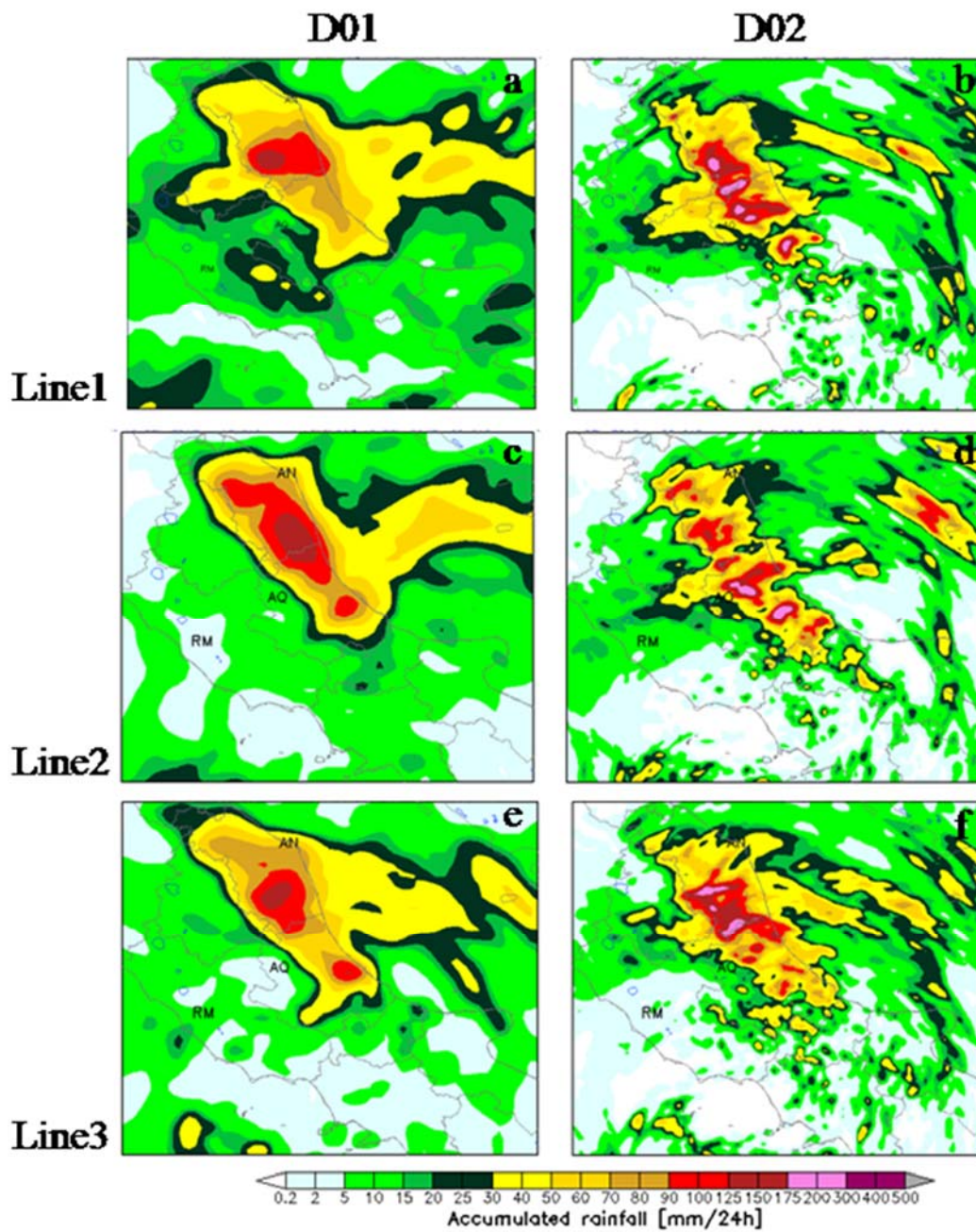
464 Figure 4: Zoom over CI of the VMI on 14 September 2012 at 08:00UTC from the Italian radar network overlapped with the
 465 MSG (IR 10.8) at 07:30UTC. (courtesy of Italian DPC)

466



467

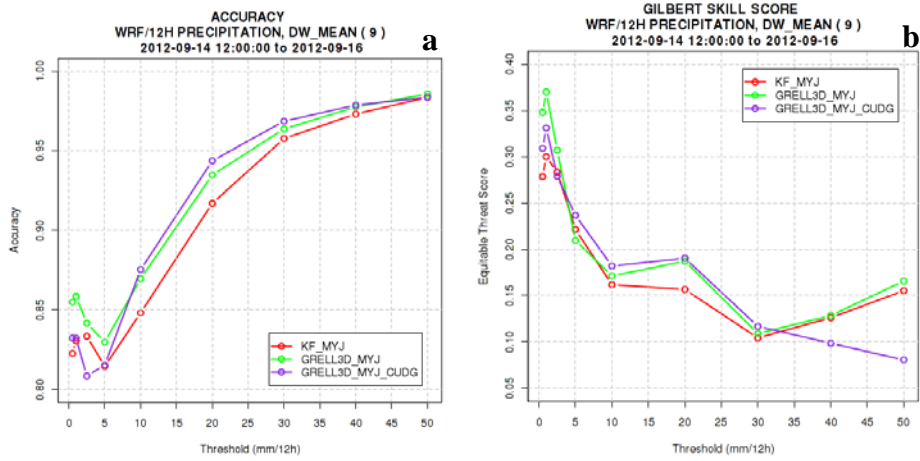
468 Figure 5: WRF nest-down domains configuration: the two domains have respectively resolution of 12 and 3 km. The high
 469 resolution D02 over Italy includes Mt. Midia (MM), ISAC-CNR (POL) and San Pietro Capofiume (SPC) radars (red dots in
 470 the figure).



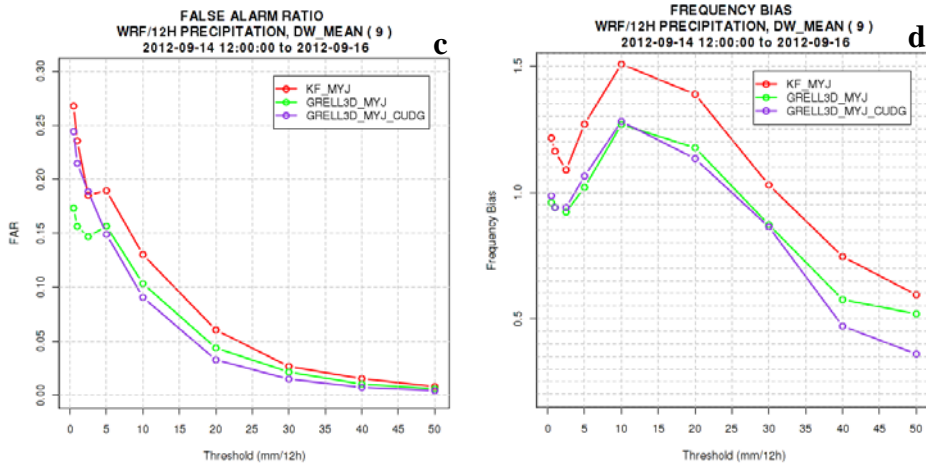
471

472 Figure 6: WRF accumulated 24h rainfall forecast on Central Italy from 00:00UTC of 14 September 2012: a,b) D01 and D02
 473 respectively run with Kain-Fritsch; c,d) D01 and D02 respectively run with Grell 3D; e,f) D01 and D02 respectively run with
 474 Grell 3D and cugd_avedx=3 activated.

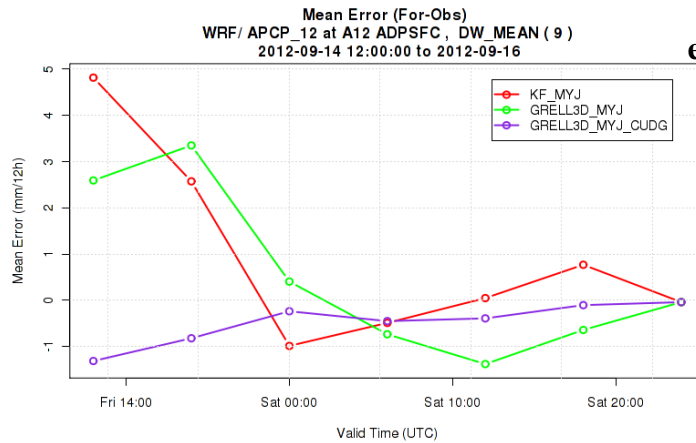
475



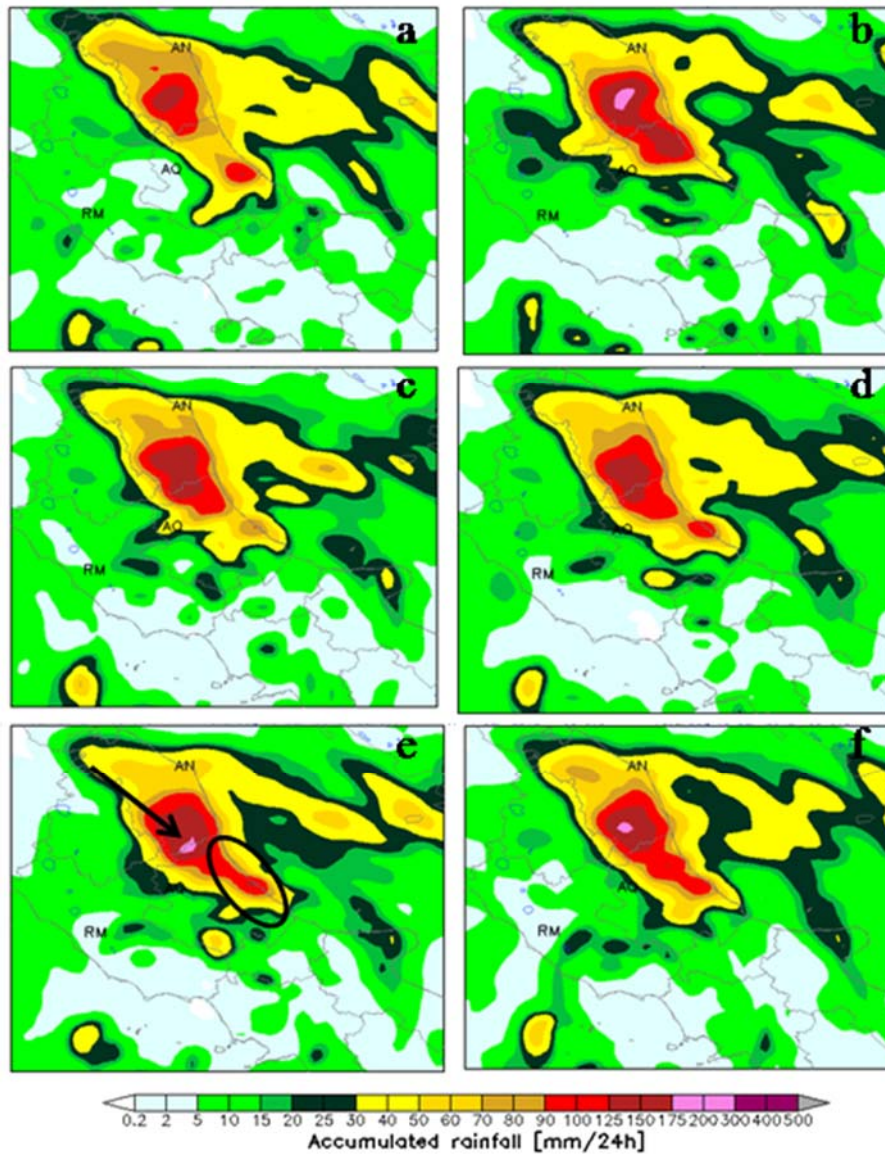
476



477



478 **Figure 7: Forecast Accuracy (a), Equitable Threat Score (b), False Alarm Ratio (c), Frequency Bias (d) as a function of**
 479 **threshold and Mean Error (e) as a function of time. The red and green curves indicate Kain-Fritsch and Grell 3D simulations**
 480 **respectively, whereas the blue curve represents Grell 3D experiment with cudg_avedx=3 activated.**

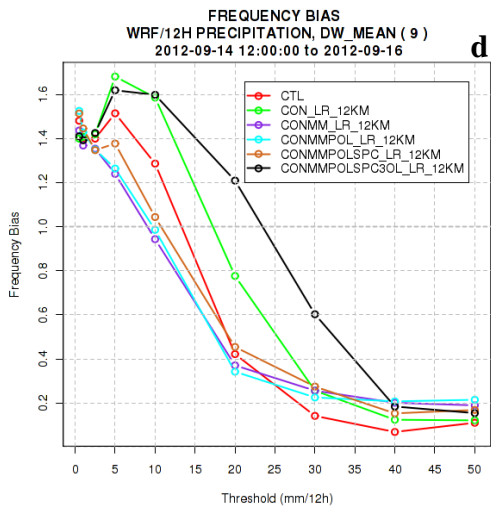
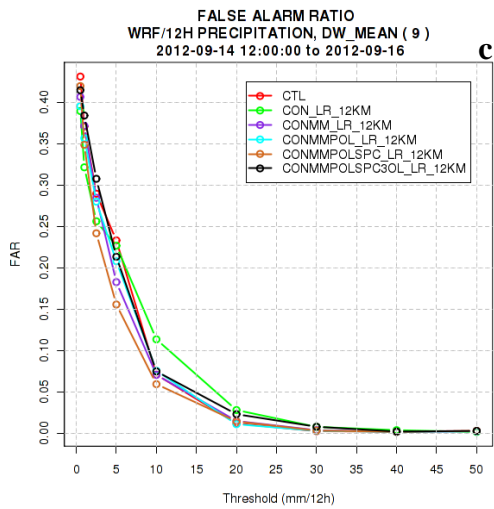
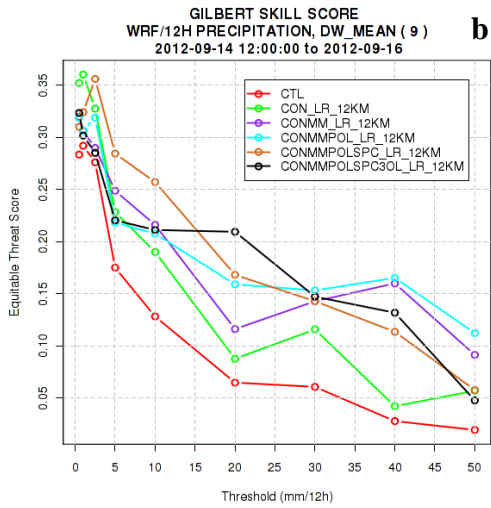
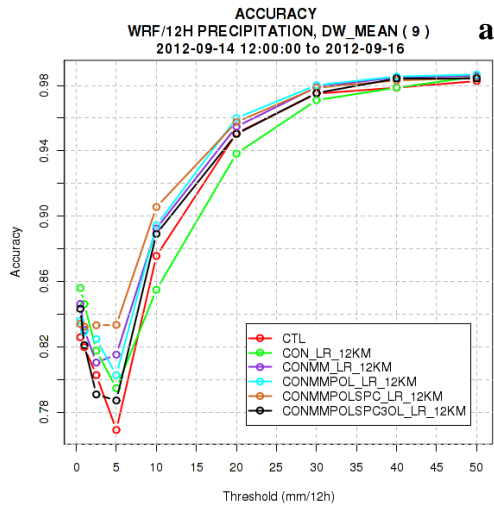


481

482 **Figure 8: WRF D01 accumulated 24h rainfall forecast on Central Italy from 00:00UTC of 14 September 2012: a) WRF D01**
 483 **CTL; b)WRF D01 CON_LR_12KM;c) WRF D01CONMM_LR_12KM;d)WRF D01CONMMPOL_LR_12KM;e) WRF**
 484 **D01CONMMPOLSPC_LR_12KM; f) WRF D01CONMMPOLSPC3OL_LR_12KM.**

485

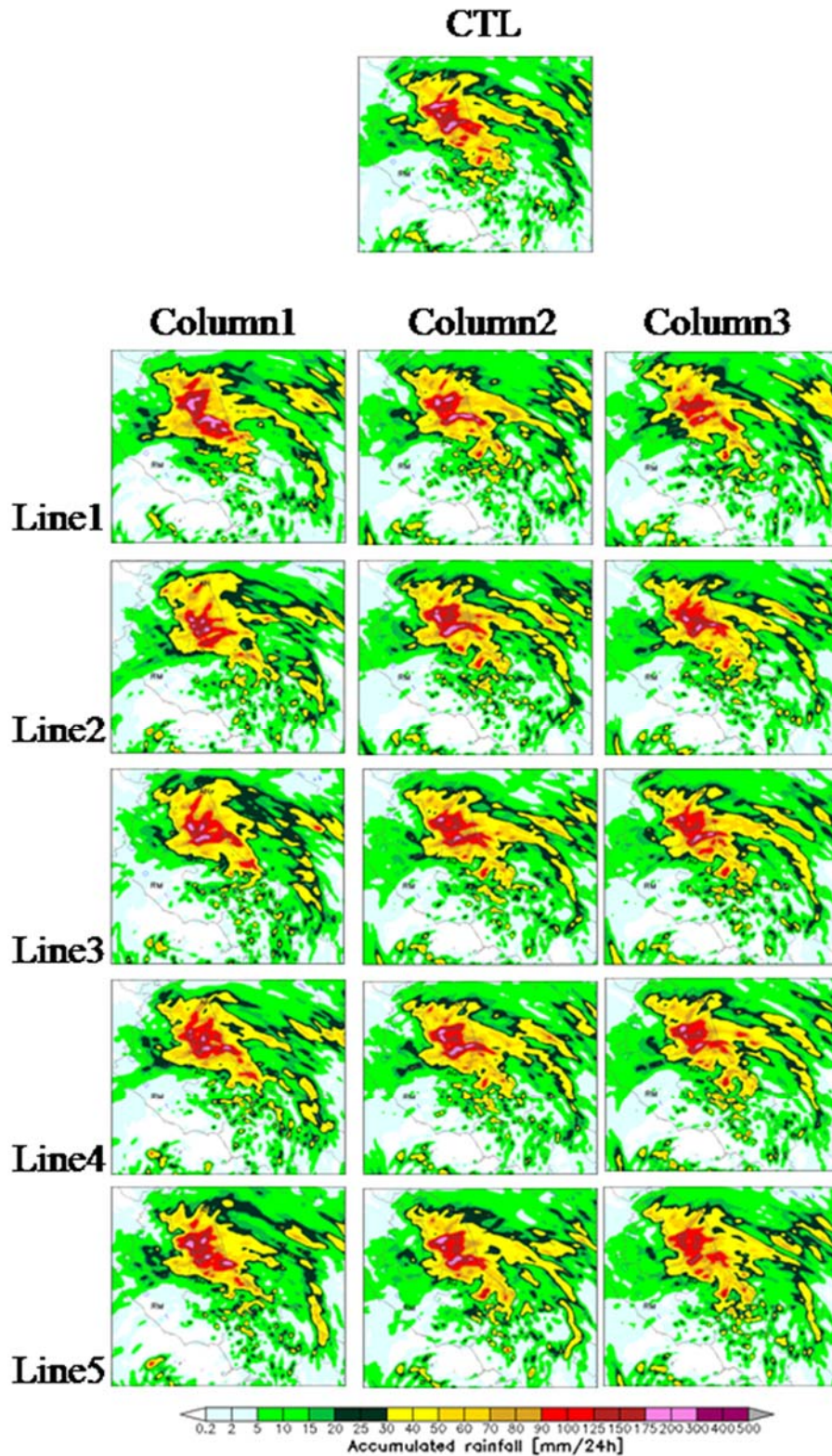
486



487

488

489 **Figure 9: Forecast Accuracy (a), Equitable Threat Score (b), False Alarm Ratio (c) and Frequency Bias (d) as a function of**
 490 **threshold. The red curve indicates CTL experiment, the green curve CON_LR_12KM, the blue curve CONMM_LR_12KM,**
 491 **the cyan curve CONMMPOL_LR_12KM, the brown curve CONMMPOLSPC_LR_12KM, the black curve**
 492 **CONMMPOLSPC3OL_LR_12KM.**



493

494 **Figure 10: WRF D02 accumulated 24h rainfall forecast on Central Italy from 00:00UTC of 14 September 2012: CTL**
 495 **simulation (top center); on each column simulations obtained performing data assimilation at different resolutions (*12KM,**
 496 ***3KM, *12KM_3KM); on each line simulations performed assimilating different kinds of data (CON*, CONMM*,**
 497 **CONMMPOL*, CONMMPOLSPC*, CONMMPOLSPC3OL*).**

498

499

500 **Table 1: List of experiments to assess the cumulus parameterization.**

Experiment	Cumulus	Grid Resolution	Assimilation Synop+Temp	Assimilation Radar
KF_MYJ	KAIN-FRITSCH	12KM/3KM	NO	NO
GRELL3D_MYJ	GRELL3D	12KM/3KM	NO	NO
GRELL3D_MYJ_CUGD (CTL)	GRELL3D+CUGD	12KM/3KM	NO	NO

501

502 **Table 2: List of experiments to test the impact of data assimilation.**

Experiment	Cumulus	Grid Resolution	Assimilation Synop+Temp	Assimilation Radar
CTL	GRELL3D+CUGD	12KM/3KM	NO	NO
CON	GRELL3D+CUGD	12KM/3KM/BOTH	YES	NO
CONMM	GRELL3D+CUGD	12KM/3KM/BOTH	YES	MM
CONMMPOL	GRELL3D+CUGD	12KM/3KM/BOTH	YES	MM+POL
CONMMPOLSPC	GRELL3D+CUGD	12KM/3KM/BOTH	YES	MM+POL+SPC
CONMMPOLSPC3OL	GRELL3D+CUGD	12KM/3KM/BOTH	YES	MM+POL+SPC with 3 outer loops

503

504

505

506

507

508

509

510

511

512 **Table 3: Statistics referred to experiments in column 1: Forecast Accuracy (ACC), Frequency Bias (FBIAS), Equitable**
 513 **Threat Score (ETS), False Alarm Ratio (FAR) are considered as a function of thresholds (1mm/12h and 20mm/12h). The**
 514 **experiments are: CTL, CON_HR_12KM, CONMM_HR_12KM, CONMMPOL_HR_12KM, CONMMPOLSPC_HR_12KM,**
 515 **CONMMPOLSPC3OL_HR_12KM.**

Experiment	ACC		FBIAS		ETS		FAR	
	Thresholds		Thresholds		Thresholds		Thresholds	
	mm/12h		mm/12h		mm/12h		mm/12h	
	1	20	1	20	1	20	1	20
CTL	0.83	0.94	0.94	1.13	0.33	0.19	0.21	0.03
CON_HR_12KM	0.81	0.93	0.91	1.12	0.25	0.17	0.26	0.04
CONMM_HR_12KM	0.82	0.94	0.95	0.99	0.28	0.17	0.24	0.03
CONMMPOL_HR_12KM	0.80	0.95	0.82	0.61	0.20	0.10	0.25	0.02
CONMMPOLSPC_HR_12KM	0.82	0.94	0.86	0.92	0.28	0.14	0.21	0.03
CONMMPOLSPC3OL_HR_12KM	0.82	0.95	0.93	0.84	0.30	0.16	0.20	0.03

516

517 **Table 4: Statistics referred to experiments in column 2: Forecast Accuracy (ACC), Frequency Bias (FBIAS), Equitable**
 518 **Threat Score (ETS), False Alarm Ratio (FAR) are considered as a function of thresholds (1mm/12h and 20mm/12h). The**
 519 **experiments are: CTL, CON_3KM, CONMM_3KM, CONMMPOL_3KM, CONMMPOLSPC_3KM,**
 520 **CONMMPOLSPC3OL_3KM.**

Experiment	ACC		FBIAS		ETS		FAR	
	Thresholds		Thresholds		Thresholds		Thresholds	
	mm/12h		mm/12h		mm/12h		mm/12h	
	1	20	1	20	1	20	1	20
CTL	0.83	0.94	0.94	1.13	0.33	0.19	0.21	0.03
CON_3KM	0.82	0.94	0.80	0.83	0.24	0.15	0.22	0.03
CONMM_3KM	0.82	0.94	0.96	0.96	0.26	0.17	0.24	0.03
CONMMPOL_3KM	0.81	0.95	0.94	0.84	0.23	0.11	0.24	0.03
CONMMPOLSPC_3KM	0.82	0.94	1.03	0.90	0.28	0.16	0.24	0.03
CONMMPOLSPC3OL_3KM	0.83	0.95	0.96	0.91	0.27	0.18	0.27	0.03

521

522 **Table 5: Statistics referred to experiments in column 3: Forecast Accuracy (ACC), Frequency Bias (FBIAS), Equitable**
 523 **Threat Score (ETS), False Alarm Ratio (FAR) are considered as a function of thresholds (1mm/12h and 20mm/12h). The**
 524 **experiments are: CTL, CON_12KM_3KM, CONMM_12KM_3KM, CONMMPOL_12KM_3KM,**
 525 **CONMMPOLSPC_12KM_3KM, CONMMPOLSPC3OL_12KM_3KM.**

526

Experiment	ACC		FBIAS		ETS		FAR	
	Thresholds		Thresholds		Thresholds		Thresholds	
	mm/12h		mm/12h		mm/12h		mm/12h	
	1	20	1	20	1	20	1	20
CTL	0.83	0.94	0.94	1.13	0.33	0.19	0.21	0.03

CON_12KM_3KM	0.81	0.95	0.84	0.73	0.20	0.14	0.27	0.02
CONMM_12KM_3KM	0.83	0.94	0.96	0.94	0.28	0.16	0.23	0.03
CONMMPOL_12KM_3KM	0.81	0.95	0.96	0.75	0.23	0.13	0.25	0.03
CONMMPOLSPC_12KM_3KM	0.81	0.95	1.04	0.79	0.26	0.17	0.28	0.02
CONMMPOLSPC3OL_12KM_3KM	0.83	0.95	0.98	0.73	0.30	0.18	0.25	0.02

527

528 **Table 6: Statistics referred to experiments in line 1: Forecast Accuracy (ACC), Frequency Bias (FBIAS), Equitable Threat**
529 **Score (ETS), False Alarm Ratio (FAR) are considered as a function of thresholds (1mm/12h and 20mm/12h). The**
530 **experiments are: CTL, CON_3KM, CON_HR_12KM, CON_12KM_3KM.**

Experiment	ACC Thresholds mm/12h		FBIAS Thresholds mm/12h		ETS Thresholds mm/12h		FAR Thresholds mm/12h	
	1	20	1	20	1	20	1	20
CTL	0.83	0.94	0.94	1.13	0.33	0.19	0.21	0.03
CON_3KM	0.82	0.94	0.80	0.83	0.24	0.15	0.22	0.03
CON_HR_12KM	0.81	0.93	0.91	1.12	0.25	0.17	0.26	0.04
CON_12KM_3KM	0.81	0.95	0.84	0.73	0.20	0.14	0.27	0.02

531

532 **Table 7: Statistics referred to experiments in line 2: Forecast Accuracy (ACC), Frequency Bias (FBIAS), Equitable Threat**
533 **Score (ETS), False Alarm Ratio (FAR) are considered as a function of thresholds (1mm/12h and 20mm/12h). The**
534 **experiments are: CTL, CONMM_3KM, CONMM_HR_12KM, CONMM_12KM_3KM.**

Experiment	ACC Thresholds mm/12h		FBIAS Thresholds mm/12h		ETS Thresholds mm/12h		FAR Thresholds mm/12h	
	1	20	1	20	1	20	1	20
CTL	0.83	0.94	0.94	1.13	0.33	0.19	0.21	0.03
CONMM_3KM	0.82	0.94	0.96	0.96	0.26	0.17	0.24	0.03
CONMM_HR_12KM	0.82	0.94	0.95	0.99	0.28	0.17	0.24	0.03
CONMM_12KM_3KM	0.83	0.94	0.96	0.94	0.28	0.16	0.23	0.03

535

536 **Table 8: Statistics referred to experiments in line 3: Forecast Accuracy (ACC), Frequency Bias (FBIAS), Equitable Threat**
537 **Score (ETS), False Alarm Ratio (FAR) are considered as a function of thresholds (1mm/12h and 20mm/12h). The**
538 **experiments are: CTL, CONMMPOL_3KM, CONMMPOL_HR_12KM, CONMMPOL_12KM_3KM.**

Experiment	ACC Thresholds mm/12h		FBIAS Thresholds mm/12h		ETS Thresholds mm/12h		FAR Thresholds mm/12h	
	1	20	1	20	1	20	1	20
CTL	0.83	0.94	0.94	1.13	0.33	0.19	0.21	0.03

CONMMPOL_3KM	0.81	0.95	0.94	0.84	0.23	0.11	0.24	0.03
CONMMPOL_HR_12KM	0.80	0.95	0.82	0.61	0.20	0.10	0.25	0.02
CONMMPOL_12KM_3KM	0.81	0.95	0.96	0.75	0.23	0.13	0.25	0.03

539

540 **Table 9: Statistics referred to experiments in line4: Forecast Accuracy (ACC), Frequency Bias (FBIAS), Equitable Threat**
541 **Score (ETS), False Alarm Ratio (FAR) are considered as a function of thresholds (1mm/12h and 20mm/12h). The**
542 **experiments are: CTL, CONMMPOLSPC_3KM, CONMMPOLSPC_HR_12KM, CONMMPOLSPC_12KM_3KM.**

Experiment	ACC Thresholds mm/12h		FBIAS Thresholds mm/12h		ETS Thresholds mm/12h		FAR Thresholds mm/12h	
	1	20	1	20	1	20	1	20
CTL	0.83	0.94	0.94	1.13	0.33	0.19	0.21	0.03
CONMMPOLSPC_3KM	0.82	0.94	1.03	0.90	0.28	0.16	0.25	0.03
CONMMPOLSPC_HR_12KM	0.82	0.94	0.86	0.92	0.28	0.14	0.21	0.03
CONMMPOLSPC_12KM_3KM	0.81	0.95	1.04	0.79	0.26	0.17	0.28	0.02

543

544 **Table 10: Statistics referred to experiments in line 5: Forecast Accuracy (ACC), Frequency Bias (FBIAS), Equitable Threat**
545 **Score (ETS), False Alarm Ratio (FAR) are considered as a function of thresholds (1mm/12h and 20mm/12h). The**
546 **experiments are: CTL, CONMMPOLSPC3OL_3KM, CONMMPOLSPC3OL_HR_12KM,**
547 **CONMMPOLSPC3OL_12KM_3KM.**

Experiment	ACC Thresholds mm/12h		FBIAS Thresholds mm/12h		ETS Thresholds mm/12h		FAR Thresholds mm/12h	
	1	20	1	20	1	20	1	20
CTL	0.83	0.94	0.94	1.13	0.33	0.19	0.21	0.03
CONMMPOLSPC3OL_3KM	0.83	0.95	0.96	0.91	0.27	0.18	0.27	0.03
CONMMPOLSPC3OL_HR_12KM	0.82	0.95	0.93	0.84	0.30	0.16	0.20	0.03
CONMMPOLSPC3OL_12KM_3KM	0.83	0.95	0.98	0.73	0.30	0.18	0.25	0.02

548